Peer-reviewed version available at *Advances in Astronomy* **2020**, *2020*, 8654307; doi:10.1155/2020/8654307

Article

Neutrino Star Cosmology

Tom F. Neiser [1,*]

[1] Department of Physics and Astronomy, University of California, Los Angeles, CA 90095, USA
* Correspondence: tomneiser@physics.ucla.edu

Abstract: The ΛCDM model successfully models the expansion of matter in the universe with an expansion of the underlying metric. However, it does not address the physical origin of the big bang and dark energy. A model of cosmology is proposed, where the state of high energy density of the big bang is created by the collapse of an antineutrino star that has exceeded its Chandrasekhar limit. To allow the first neutrino stars and antineutrino stars to form naturally from an initial quantum vacuum state, it helps to assume that antimatter has negative gravitational mass. While it may prove incorrect, this assumption may also help identify dark energy. The degenerate remnant of an antineutrino star can today have an average mass density that is similar to the dark energy density of the ΛCDM model. When in hydrostatic equilibrium, this antineutrino star remnant can emit isothermal cosmic microwave background radiation and accelerate matter radially. This model and the ΛCDM model are in similar quantitative agreement with supernova distance measurements. Other observational tests of the above model are also discussed.

Keywords: cosmology; big bang; dark energy; neutrinos; gravitation

1. Introduction

Type-Ia supernovae (SNe Ia) occur when an accreting white dwarf star exceeds the Chandrasekhar limit and collapses until the released potential energy detonates the star with carbon fusion. Due to their similar initial conditions, SNe Ia can serve as standard candles. Twenty years ago, this allowed observations of SNe Ia to show an accelerating expansion of matter on cosmological scales [1–3]. The big bang model successfully describes this expansion with an expansion of the underlying metric. It assumes that the universe is homogeneous and isotropic on large scales, which is known as the cosmological principle. Mathematically, the Friedman-Lemaître-Robertson-Walker (FLRW) metric upholds the cosmological principle by uniformly changing the metric of space with a scale factor that varies in time. Today, a concordance from various observations defines the ΛCDM model, which divides the energy content of the universe into 31% matter and 69% dark energy, where dark energy is commonly thought to be the constant energy density of the quantum vacuum [4,5]. This translates to a dark energy density of $\rho_\Lambda \approx 6 \times 10^{-30}\mathrm{g/cm}^3$, which is 10^{120} times smaller than expected [6]. Therefore the identity of dark energy is a major unsolved puzzle. Alternative models posit a negative gravitational mass [7–10], negative inertial mass [11] or relic neutrino condensation [12,13]. Despite these alternatives, the ΛCDM model is so far our most successful description of the late universe.

While the ΛCDM model is the most widely accepted model of the late universe, it does not address several key puzzles associated with the early universe. First, when we trace the expansion of all observable matter ($\sim 10^{55}$ g) backwards in time, we encounter a collective state of high energy density that is associated with the big bang. Current models treat the big bang either as the beginning of space and time [14], or as part of a continuous bounce [15,16]. While it serves as initial condition for the ΛCDM model, the origin of the big bang is a major unsolved puzzle. A second problem arises when we assume that this big bang state initially contained equal amounts of matter and antimatter, while unequal amounts are observed in the universe today. To account for this matter-antimatter asymmetry, it is necessary to find a mechanism for baryogenesis [17,18]. A third puzzle is associated with the cosmic microwave background radiation (CMB). The ΛCDM model assumes that the CMB

was emitted by initially hot and dense matter that has cooled sufficiently to become transparent to radiation $\sim 10^5$ years after the big bang [19]. However, the CMB is more isotropic than expected, which is known as the horizon problem. The theory of cosmological inflation addresses this by introducing a period of exponentially accelerating expansion up to 10^{-32} s after the big bang [20–22]. This could allow any two regions of the CMB in the early universe to have been thermalized. This also addresses the question of why our expanding metric appears to be spatially flat, known as the flatness problem. However, inflation suffers from problems such as the entropy problem or the multiverse problem [23,24]. Lastly, the standard model interpretation of the CMB appears to be in tension with recent cosmology-independent measurements of the expansion rate at both low redshifts ($z < 0.15$) and high redshifts ($1.4 < z < 5.1$) at the $\sim 4\sigma$ level [25–27]. These puzzles motivate a search for new models, with the ΛCDM model as the benchmark.

In the present work, a model of cosmology is proposed that attempts to address the origin of the big bang and dark energy. A degenerate self-gravitating gas of antineutrinos, which we will call an antineutrino star, collapses when its mass exceeds the Chandrasekhar limit, $\mathcal{M}_{\nu_e} \propto 1/m_{\nu_e}^2$ [28,29]. The small neutrino mass (m_{ν_e}) motivates a model of cosmology, where the collapse of an antineutrino star creates the state of high energy density of the big bang with a minimum of new physics. As initial condition of the proposed model, we choose a quantum vacuum state due to its minimal entropy. This state is gravitationally unstable and organically forms spatially separated neutrino stars and antineutrino stars when we assume that antimatter has negative gravitational mass. After collapse in an energetic event as described below, a fraction of the antineutrino gas eventually returns to effective hydrostatic equilibrium. If viewed from the core, a degenerate antineutrino star remnant could today emit isothermal cosmic microwave background radiation and radially accelerate matter.

The main finding is that both the new model and the ΛCDM model describe redshift-distance measurements with comparable quantitative accuracy. The best-fit parameters of the new model give a density of the antineutrino star that is similar to the dark energy density of the ΛCDM model, and constrain the electron neutrino mass to high statistical precision. The new model is qualitatively consistent with CMB anisotropies [30] and large-scale structures [31,32], which presently challenge the ΛCDM model's assumptions of homogeneity and isotropy. These results encourage future work to further develop and test the presented model.

2. Antineutrino star model of the early universe

Similar to a white dwarf star, a degenerate gas of antineutrinos collapses when its mass exceeds the Chandrasekhar limit. In this section we will show that this collapse can transform energy at the scale of the mass-energy content of the known universe. In order to create the conditions for this event to occur, it becomes helpful to assume that antimatter has negative gravitational mass. This assumption is currently being tested at CERN, and, if true, may also help describe dark energy.

2.1. Chandrasekhar's equation of state

To characterize a degenerate antineutrino gas in effective hydrostatic equilibrium, we first make three assumptions. First, we ignore thermal or radiation pressure of the antineutrino gas by assuming it is highly degenerate with temperature $T/T_\mathrm{F} \ll 1$, where T_F is the Fermi temperature. Second, we assume that the neutrino is a Dirac fermion, which means that it is not its own antiparticle. This standard model assumption is being tested by the search for neutrinoless double-beta decay [33,34]. Third, we assume that all neutrinos in the star are electron flavored neutrinos with effective inertial mass m_{ν_e}. Note that due to neutrino oscillations [35,36], free electron neutrinos have an effective mass $m_{\nu_e} = \sum_i |U_{ei}|^2 m_i$, where U_{ei} are the Pontecorvo–Maki–Nakagawa–Sakata leptonic mixing matrix elements and m_i are eigenstates of definite mass ($i = 1, 2, 3$, respectively). We will show that this third assumption is reasonable in the context of the Schwinger mechanism (see Eq. 19) if the electron neutrino mass m_{ν_e} is much less than the muon (m_{ν_μ}) or tau (m_{ν_τ}) neutrino masses.

With these assumptions we can use Chandrasekhar's equation of state for degenerate matter, derived from hydrostatic equilibrium of gravitational and degeneracy pressures [28,29,37]. We thus get the equations of density,

$$\rho = \frac{K}{c^2}\left[x\sqrt{1+x^2}\left(1+2x^2\right) - \ln\left(x+\sqrt{1+x^2}\right)\right], \tag{1}$$

and pressure,

$$P = K\left[x\sqrt{1+x^2}\left(\frac{2}{3}x^2-1\right) + \ln\left(x+\sqrt{1+x^2}\right)\right], \tag{2}$$

where x is dimensionless and proportional to the Fermi momentum p_{F},

$$x = \frac{p_{\mathrm{F}}}{m_{\nu_e}c}, \tag{3}$$

and K has dimensions of energy density,

$$K = \frac{m_{\nu_e}^4 c^5}{8\pi^2\hbar^3}. \tag{4}$$

We want to solve the following equation for hydrostatic equilibrium,

$$\frac{dP}{dr} = -\rho\frac{Gm(r)}{r^2}, \tag{5}$$

where $m(r)$ is the gravitational mass enclosed inside a radius r and is given by

$$\frac{dm}{dr} = 4\pi r^2\rho(r). \tag{6}$$

The spherically symmetric gravitational potential $\varphi(r)$ is given by

$$\frac{d\varphi}{dr} = \frac{Gm(r)}{r^2}. \tag{7}$$

For regions outside an antineutrino star ($r > R$) the potential simplifies to

$$\varphi(r) = \varphi(R) - GM\left(\frac{1}{r}-\frac{1}{R}\right), \tag{8}$$

where $M < 0$ is the gravitational mass of the antineutrino star. The radius R of the star can be found where $P(R) = 0$, while the total mass of the star is given by $M = m(R)$,

$$M = 4\pi\int_0^R \rho(r)r^2\,dr. \tag{9}$$

Chandrasekhar's equation of state above does not take into account general relativistic effects, which we can ignore for simplicity if the radius of the star is much larger than its Schwarzschild radius, $R_S/R \ll 1$. Note that we assume that inertial masses ($m_i = |m|$) of matter and antimatter are equal and positive, and that the gravitational mass ($m_g = m$) of matter is positive ($m_g/m_i = 1$) and of antimatter is negative ($m_g/m_i = -1$); for generality, we don't use overbar notation. Note that the gauge is fixed to zero at the star's center, $\varphi(0) = 0$, so that $\varphi(r) < 0$ everywhere else.

The above equations can be solved numerically for a given central density ρ_0 and effective neutrino mass m_{ν_e}. To facilitate this, we recast equations (5-7) above using dimensionless units for radial position $\eta = r/a$, mass $\mu = m/b$, and potential $\phi = \varphi/c^2$, where

$$a = \left(\frac{2\pi\hbar^3}{Gc}\right)^{1/2}\left(\frac{1}{m_{\nu_e}}\right)^2, \tag{10}$$

Preprints (www.preprints.org) | NOT PEER-REVIEWED | Posted: 28 October 2019 doi:10.20944/preprints201806.0175.v2

Peer-reviewed version available at Advances in Astronomy 2020, 2020, 8654307; doi:10.1155/2020/8654307

$$b = \sqrt{2\pi}\left(\frac{\hbar c}{G}\right)^{3/2}\left(\frac{1}{m_{\nu_e}}\right)^2, \tag{11}$$

and the other constants take their usual meaning. This gives for hydrostatic equilibrium

$$\frac{dx}{d\eta} = -\frac{3\left(x+3x^3+2x^5-\sqrt{1+x^2}\,\mathrm{arcsinh}\,x\right)}{8x^4}\frac{\mu}{\eta^2}, \tag{12}$$

and for the mass enclosed

$$\frac{d\mu}{d\eta} = \eta^2\left[x\sqrt{1+x^2}\left(1+2x^2\right)-\ln\left(x+\sqrt{1+x^2}\right)\right], \tag{13}$$

while the potential becomes

$$\frac{d\phi}{d\eta} = \frac{\mu}{\eta^2}. \tag{14}$$

Using the boundary conditions $\mu(0) = 0$, central density $x(0) = x_0$ and fixing the gauge $\phi(0) = 0$ allows us to solve the above three equations. For illustrative purposes, the mass-radius relationship for an antineutrino star is plotted in Fig. 1. The constants a and b depend on the neutrino mass as follows,

$$a = 25.6 \text{ billion lightyears (Gly)} \times \left(\frac{5\,\mathrm{meV}}{m_{\nu_e}c^2}\right)^2, \tag{15}$$

$$b = 3.25\times 10^{56}\mathrm{g}\times\left(\frac{5\ \mathrm{meV}}{m_{\nu_e}c^2}\right)^2. \tag{16}$$

These large scale factors suggest that neutrino stars and antineutrino stars may be relevant for cosmology [38].

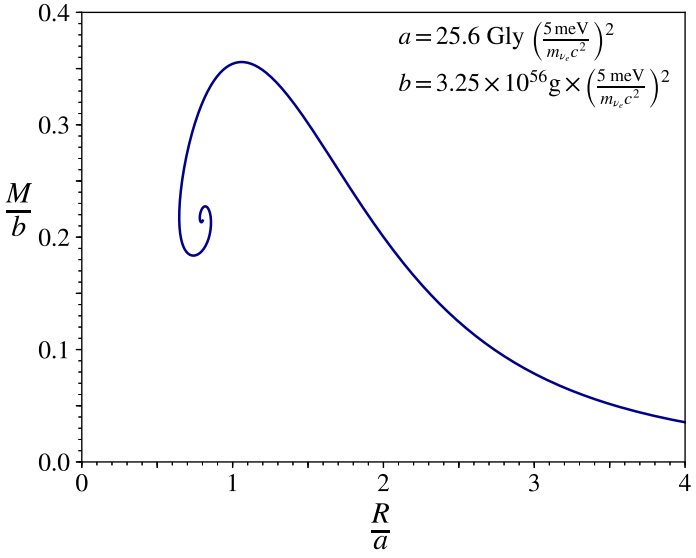

Figure 1. Mass-radius relationship for a neutrino star. The peak occurs at $R/a = 1.06$ and $M/b = 0.356$, which for neutrinos of mass $m_{\nu_e} = 5.0$ meV/c^2 corresponds to $R = 27$ billion lightyears (Gly) and $M = 1.16\times 10^{56}$ g. At smaller radii, the mass-radius curve corresponds to unstable configurations. Therefore neutrino stars may be relevant for cosmology.

2.2. Chandrasekhar limit

The estimated mass-energy content of the universe at the time of the big bang is $\sim 10^{55}$ g [5]. In the early universe, this mass-energy was concentrated in a state of high energy density. Possible origins of the big bang have been discussed by several authors [14–16]. One possibility, which seems to have been overlooked in earlier discussions, is that the big bang was created by the gravitational collapse of an antineutrino star. When a white dwarf star exceeds the Chandrasekhar limit, its own gravitational pressure overwhelms the degeneracy pressure of electrons and it collapses in a supernova [28]. Similarly, the limiting mass of a degenerate gas of electron antineutrinos occurs at the dimensionless values of $\eta = 1.06$ and $\mu = 0.356$, which corresponds respectively to

$$\mathcal{R}_{\nu_e} = 27.1 \text{ Gly } \times \left(\frac{5 \text{ meV}}{m_{\nu_e} c^2} \right)^2 , \tag{17}$$

$$\mathcal{M}_{\nu_e} = 1.16 \times 10^{56} \text{g} \times \left(\frac{5 \text{ meV}}{m_{\nu_e} c^2} \right)^2 . \tag{18}$$

The electron neutrino mass was recently constrained to $m_{\nu_e} < 1.1 \text{ eV}/\text{c}^2$ by the KATRIN experiment [39, 40]. This gives a lower limit of $\mathcal{M}_{\nu_e} > 2.39 \times 10^{51}$ g, which is only four orders of magnitude below the estimated mass-energy content of the universe at the time of the big bang ($\sim 10^{55}$ g). Moreover, an effective electron neutrino mass of $m_{\nu_e} = 5 \text{ meV}/\text{c}^2$ would correspond to a Chandrasekhar limit of $\mathcal{M}_{\nu_e} = 1.16 \times 10^{56}$ g. Due to these cosmological length and mass scales, the study of neutrino stars and antineutrino stars falls within the realm of cosmology [38]. A small neutrino mass motivates the ansatz of this paper that the collapse of an antineutrino star created the state of high energy density of the big bang with a minimum of new physics.

2.3. Quantum vacuum instability

The hypothesis that the collapse of an antineutrino star created the state of high energy density of the big bang immediately raises the question on the origin of the first neutrino stars and antineutrino stars. We attempt to address this qualitatively in the following and warn the reader that this subsection and the next subsection are more speculative than the others. Before the first neutrino and antineutrino stars are formed, it is reasonable to assume that the initial condition of the universe was an infinite volume of quantum vacuum due to its low number of degrees of freedom. The quantum vacuum contains a sea of virtual particle-antiparticle pairs going into and out of existence. The universe today is no longer in this low-entropy quantum vacuum state. To explain this, we assume that matter and antimatter gravitationally repel, which causes the quantum vacuum to be gravitationally unstable by the following mechanism. Short-lived perturbations in the particle-antiparticle density create a weak and fluctuating gravitational field on small scales (this field is established by the particles themselves). By the Schwinger mechanism, this field has a *non-zero* probability of creating real particles by separating virtual ones before they can annihilate [9,41]. For example, the pair creation rate per unit volume and time in a constant local gravitational field gradient, g, is

$$\frac{dN}{dtdV} = \frac{m^4 c^5}{4\pi\hbar^4} \left(\frac{\hbar |g|}{\pi m c^3} \right)^2 \sum_{n=1}^{\infty} \frac{1}{n^2} \exp\left(-n \frac{\pi m c^3}{\hbar |g|} \right) . \tag{19}$$

According to the above equation, even the weak and fluctuating gravitational field of particles in the quantum vacuum can create real particles with non-zero probability. The exponential dependence on the effective mass (m) strongly favors creation of neutrino-antineutrino pairs compared to more massive particles of the Standard Model [9,42]. It also favors cold neutrinos over hot neutrinos, which allows them to bind gravitationally. Thus, the assumption of negative gravitational mass of antimatter enables the gradual formation of mutually repulsive neutrino stars and antineutrino stars.

2.4. Qualitative description of the collapse of an antineutrino star

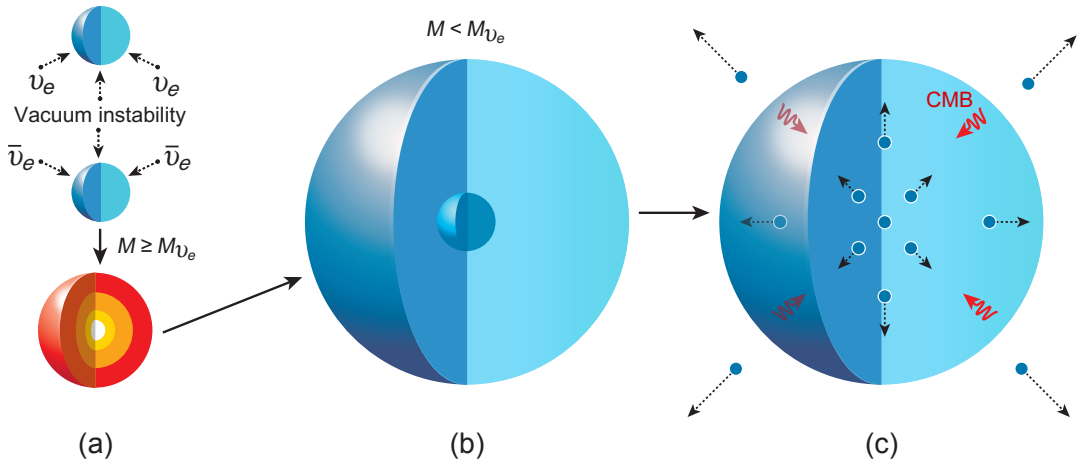

Figure 2. Summary schematic of the ATLAS model. (a) Assuming that antimatter has negative gravitational mass, the quantum vacuum is unstable and forms spatially separated neutrino stars and antineutrino stars. An antineutrino star collapses in a neutrinonova when its mass exceeds the Chandrasekhar limit. A large fraction of the kinetic energy released in the collapse converts to baryons and antibaryons. After baryogenesis and nucleosynthesis, the surviving baryons and antineutrinos expand adiabatically. (b) Structure formation begins in a much smaller volume for baryons (*inner sphere*) than for antineutrinos (*outer sphere*). (c) The antineutrino star remnant returns to hydrostatic equilibrium, emits isothermal cosmic microwave radiation and radially accelerates matter. If we are close to the core, this model could explain the overall expansion of matter.

Whenever an accreting antineutrino star exceeds its mass limit, it collapses in a "neutrinonova". At sufficiently high temperatures and densities, antineutrinos could transform most of their kinetic energy via high-energy collisions into equal quantities of baryonic matter and antimatter. This is qualitatively similar to the conversion of large amounts of kinetic energy into equal quantities of matter and antimatter in experiments such as the Large Hadron Collider at CERN. The collapse could subsequently be reversed in a big bounce. While the details of the bounce mechanism are unknown at this point, they would likely involve nuclear fusion and other physical processes similar to the bounce event of supernovae.

During the subsequent expansion of material, baryonic matter and antimatter start to annihilate faster than they are created. We assume that a small remnant of baryonic matter survives due to baryogenesis [17,18]. Similar to a supernova bounce, a fraction of the original antineutrino star is accelerated to escape velocities from the shock wave associated with the bounce. The remaining antineutrinos and matter expand as two adiabatic ideal gases initially in thermal equilibrium. During adiabatic expansion, the temperature (T) decreases with an increase in volume (V) as $T \propto V^{-1/3}$ for a relativistic gas and $T \propto V^{-2/3}$ for a non-relativistic gas. Thus, baryonic matter undergoes nucleosynthesis until density and temperature decrease sufficiently to "freeze out" certain reactions. This process could produce light elements comparable to big bang nucleosynthesis (BBN) [43]. Note that a neutrinonova is not associated with an expansion of the underlying metric, but an expansion of material (as in a supernova). Since baryonic particles are much more massive than antineutrinos, they become non-relativistic at a much higher temperature than antineutrinos, and thus begin structure formation in a much smaller volume. The antineutrinos that have not been accelerated to escape velocities eventually form a degenerate self-gravitating gas with sub-Chandrasekhar mass ($M < \mathcal{M}_{\nu_e}$), and re-establish thermal equilibrium a sufficient time afterwards ($t \gg R/c$). Newly formed galaxies are subsequently radially accelerated from initial proximity to the center of the antineutrino star

remnant. Observers in the rest frame and inside of this antineutrino star in hydrostatic equilibrium would detect isotropic black body radiation, which we identify as the CMB. We call this the ATLAS (AnTineutrino Lepton gAS) model[1] and refer to the antineutrino star as ATLAS-1 (see Fig. 2 for a summary).

To summarize this section, the collapse of an antineutrino star can explain the energetic event commonly known as the big bang. It suggests that an antineutrino star remnant in hydrostatic equilibrium may exist in the universe today. This degenerate antineutrino star is detectable by isothermal background radiation and the large-scale motion of galaxies. In the following section we quantitatively show that this antineutrino star remnant could account for the large-scale motion of galaxies with similar accuracy as the ΛCDM model.

3. Antineutrino star model of the late universe

The ΛCDM model can mathematically describe the large-scale motion of galaxies with only two parameters, the fractional matter density (Ω_m) and dark energy density (Ω_Λ). As we will show below, an antineutrino star model can describe the large-scale motion of galaxies competitively in the contingency that ongoing experiments at CERN discover negative gravitational mass. The equation of state of an antineutrino star is defined by two unknown parameters, namely the central density (ρ_0) and the effective electron neutrino mass (m_{ν_e}). An initial average expansion velocity of baryonic matter (v_0) as a third parameter improves the physical basis of our model at low redshifts ($z < 0.04$) and could qualitatively explain the 4.4σ Hubble tension [25,26].

3.1. Definition of our observational frame

An antineutrino star establishes a background potential that is the dominant contribution to the apparent velocities of galaxies. Therefore, we can infer our approximate position empirically from our velocities relative to other galaxies and relative to the rest frame of the antineutrino star, which is the rest frame of the CMB. The velocities of galaxies relative to us scale approximately *isotropically* with distance at a rate of $H_0 \approx 70$ km s^{-1}Mpc^{-1} [25,26]. The velocity of the Local Group relative to the CMB is comparably small at $v_{CMB} \approx 627$ km s^{-1} [44]. These velocities suggest we are approximately at rest and near (but not at) the center of the star. This can be physically explained by the small potential gradient near the center, which causes matter initially close to the center to remain effectively at rest, while matter far from the center accelerates down the gravitational potential hill at an apparent rate of H_0. This empirical inference of our observational frame guides our derivation of the distance redshift-relationship below.

3.2. Derivation of a distance-redshift relationship

We will use the Schwarzschild metric to determine the redshift of light emitted by a galaxy in free fall from initial proximity to the center of an antineutrino star. We may identify ourselves as Schwarzschild observers, who are by definition at rest where the gauge is fixed to zero, namely at the star's center. When allowing for negative gravitational mass, we need to define two different metrics for matter and for photons.

By symmetry, we assume that photons in a gravitational potential undergo blueshift or redshift independently of the matter or antimatter nature of the gravitational source. We will thus use a Schwarzschild metric for photons that is agnostic to the type of matter,

$$d\tau_\gamma^2 = \left(1 + \frac{2\varphi(r)}{c^2}\frac{M}{|M|}\right) dt_\gamma^2 - \frac{dr_\gamma^2}{c^2}\frac{1}{1 + \frac{2\varphi(r)}{c^2}\frac{M}{|M|}} - \frac{r^2 d\Omega_\gamma^2}{c^2}, \tag{20}$$

[1] In Greek mythology Atlas is a titan who holds up the celestial spheres.

where $M/|M|$ is the sign of the gravitational mass of the source, t is coordinate time, $d\Omega^2 = \sin\theta^2 d\phi^2 + d\theta^2$ is the angular path element in spherical coordinates, and $\varphi(r)$ is the gravitational potential of the antineutrino star given by equations (7) and (8). Note that the above equation is only an approximation of the metric inside the star ($r < R$), since we used Chandrasekhar's Newtonian model for simplicity to find $\varphi(r)$. It is worth repeating here that this approximation is accurate when changes in gravitational potential inside the star satisfy $2|\varphi(r)|/c^2 \ll 1$. Outside of the star ($r > R$), the above Schwarzschild metric accurately captures all *further* changes in gravitational potential relative to the central observer up to $2|\varphi(r)|/c^2 \lesssim 1$.

Since proper time is zero for photons, the velocity $v_\gamma = (dr/dt)_\gamma$ of distant photons moving radially ($d\Omega_\gamma = 0$) is

$$\frac{v_\gamma}{c} = 1 + \frac{2\varphi(r)}{c^2}\frac{M}{|M|}\,. \tag{21}$$

To summarize the above result, photons are assumed to behave in a way that is agnostic to the matter or antimatter nature of the gravitational source.

We assume that matter experiences a Schwarzschild metric that has been minimally extended to capture the interaction of negative and positive gravitational masses

$$d\tau^2 = \left(1 + \frac{2\varphi(r)}{c^2}\frac{m}{|m|}\right)dt^2 - \frac{dr^2}{c^2}\frac{1}{1 + \frac{2\varphi(r)}{c^2}\frac{m}{|m|}} - \frac{r^2 d\Omega^2}{c^2}\,, \tag{22}$$

where $m/|m|$ is the sign of the gravitational mass of a test particle. Note that the above expression allows matter and antimatter to experience two different space-time metrics that are equal where the gauge is fixed to zero.

We can now use energy conservation [45] to find the time dilation factor for galaxies with average initial velocity v_0 undergoing free fall from the center of the star,

$$\frac{d\tau}{dt} = \left(1 + \frac{2\varphi(r)}{c^2}\frac{m}{|m|}\right)\sqrt{1 - \frac{v_0^2}{c^2}}\,. \tag{23}$$

The coordinate velocity $v_s = dr/dt$ is found similarly [45],

$$\frac{v_s}{c} = \left(1 + \frac{2\varphi(r)}{c^2}\frac{m}{|m|}\right)\sqrt{\frac{v_0^2}{c^2} - \left(1 - \frac{v_0^2}{c^2}\right)\frac{2\varphi(r)}{c^2}\frac{m}{|m|}}\,. \tag{24}$$

The above equations allow us to calculate the redshift seen by a Schwarzschild observer,

$$z = \left(\frac{dt}{d\tau}\right)\left(1 + \frac{v_s}{v_\gamma}\right) - 1\,. \tag{25}$$

Therefore, redshift is caused by a combination of apparent radial velocity v_s and time dilation of free-falling sources in the gravitational potential φ. Specifically, contributions of v_s to redshift dominate at low-z and contributions from $\varphi(r)$ via time dilation dominate at high-z (this will also be shown graphically in Fig. 4). The distance modulus of distant SNe Ia in receding galaxies is

$$\mu_{\rm th}(z) = 25 + \log_{10}[r(z)(1+z)]\,, \tag{26}$$

where $r(z)$ is the distance from the center of the antineutrino star in Megaparsec [1].

3.3. Cosmological Parameters

We can compare the theoretical distance modulus to observed distance moduli for a given set of cosmological parameters, $\theta = (m_{\nu_e}, \rho_0, v_0)$. Goodness of fit is determined with a χ^2 statistic,

$$\chi^2_\nu(\theta) = \sum_i \frac{[\mu_{\mathrm{th},i}\,(z_i;\theta) - \mu_{0,i}(z_i)]^2}{\sigma^2_{\mu_{0,i}}}\,, \tag{27}$$

where $\sigma_{\mu_{0,i}}$ is the measurement uncertainty in the observed distance modulus $\mu_{0,i}$. As observational data, the "Union2.1" catalog[2] of 580 SNe Ia is used [46]. The best-fit parameter values are $m_{\nu_e} = 6.70$ meV/c^2, $\rho_0 = 1.60 \times 10^{-29}$ g/cm^3 and $v_0 = 6.18 \times 10^{-3}c$. These give $\chi^2_\nu/\mathrm{dof} = 1.03$, where dof stands for a model's degrees of freedom. For reference, the ΛCDM model has a comparable fit of $\chi^2_\Lambda/\mathrm{dof} = 1.09$ [5]. In Figure 3 the theoretical distance modulus of the ATLAS model with the above best-fit parameters is plotted together with the distance-redshift data in a Hubble diagram. For

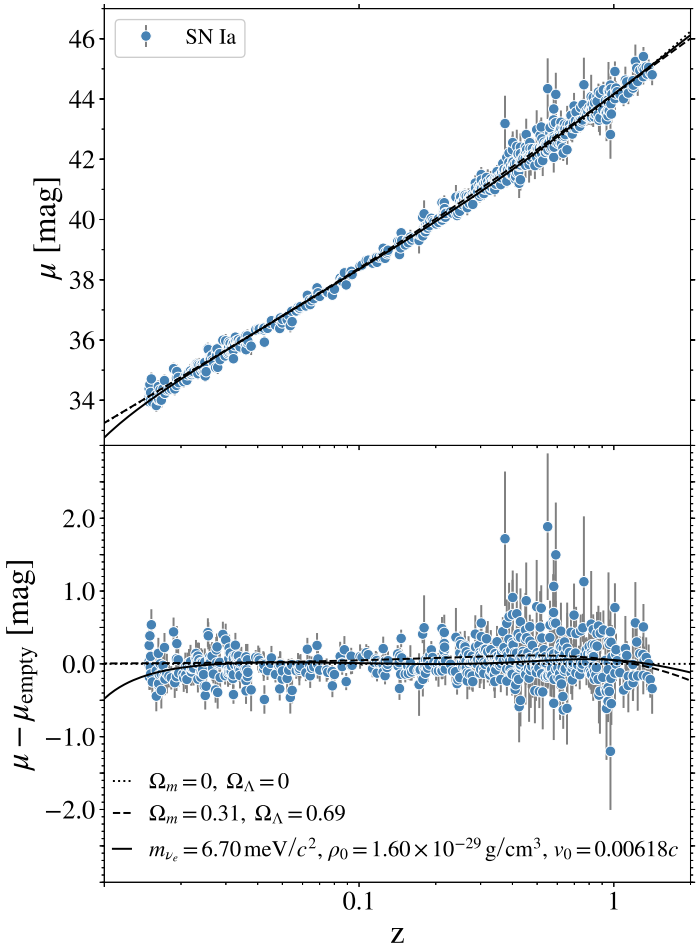

Figure 3. *Top*: Hubble diagram of 580 SNe Ia (*circles*) from the Union catalog [46] with comparable fits by the ΛCDM model (*dashed line*) and the ATLAS model (*solid line*). *Bottom*: Hubble diagram relative to the empty universe model for a better comparison. The difference between the two models at $z < 0.04$ is created by the assumption of an initial average expansion velocity of galaxies (v_0), which could qualitatively explain the 4.4σ Hubble tension [25,26]. Note that the central density ρ_0 is quantitatively comparable to the dark energy density of the ΛCDM model ($\rho_\Lambda \approx 6 \times 10^{-30}$g/cm^3 [5]).

comparison, the theoretical distance modulus of the concordance ΛCDM model [5] is shown with $H_0 = 67.74$ km s^{-1}Mpc^{-1}. Note that the central density of the antineutrino star ρ_0 is comparable to the dark energy density of the ΛCDM model. Therefore the ATLAS model can account for the overall

[2] http://supernova.lbl.gov/union/; date accessed: 08/09/2017

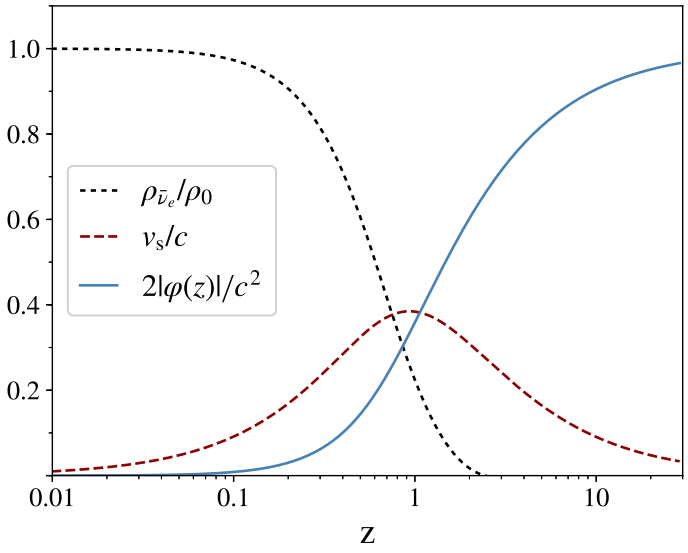

Figure 4. Density-redshift profile, and relative contributions to the redshift by gravitational potential and radial velocity. In the ATLAS model, redshifts at low-z are mainly due to radial velocity (*dashed curve*) and at high-z due to time dilation of free-falling sources in the gravitational potential φ (*solid curve*). The density (*dotted curve*) acts as a form of dark energy density and vanishes at the antineutrino star's radius, $R = 21.1$ Gly (or $z = 2.49$).

expansion of matter, with the density profile of an antineutrino star in equilibrium effectively acting as a spatially varying dark energy density (see Fig. 4).

Following Riess *et al.* [1], the probability density function (PDF) for a given cosmological parameter is quantified with Bayes' theorem, which gives a PDF for the electron neutrino mass of

$$p(m_{\nu_e}|\mu_0) = \frac{\int_0^c dv_0 \int_0^\infty \exp(-\chi^2/2)\, d\rho_0}{\int_0^c dv_0 \int_0^\infty d\rho_0 \int_0^\infty \exp(-\chi^2/2)\, dm_{\nu_e}}, \tag{28}$$

where μ_0 represents all measured distance moduli, which are assumed to be independent and normally distributed. This gives a mass to one standard deviation of $m_{\nu_e} = 6.70 \pm 0.23$ meV/c^2 (see Fig. 5). Note that this uncertainty is purely due to statistical error and does not include possible systematic errors, which can be caused by model assumptions or instrument calibration [46]. This mass is consistent with the present experimental upper limit of $m_{\nu_e} < 1.1$ eV/c^2 [40], and may be tested by future or ongoing experiments. Measurements of neutrino mixing angles can give the muon and tau neutrino masses: for example, the most recent[3] best-fit values give $[m_{\nu_\mu}, m_{\nu_\tau}] \approx [30.1, 26.4]$ meV/c^2 [47].

4. Discussion

The antineutrino star parameters are approximately consistent with the assumptions of the ATLAS model. The best-fit muon and tau neutrino masses are larger than the electron neutrino mass by a factor of > 3. This is consistent with the simplifying assumption that the antineutrino star consists only of electron neutrinos due to the Schwinger mechanism (see section 2.1). The best-fit electron neutrino mass (m_{ν_e}) gives a Chandrasekhar limit of

$$\mathcal{M}_{\nu_e} = 6.45 \times 10^{55}\ \text{g}, \tag{29}$$

[3] NuFIT 3.2 (2018), http://www.nu-fit.org/?q=node/166; date accessed: 06/07/2018

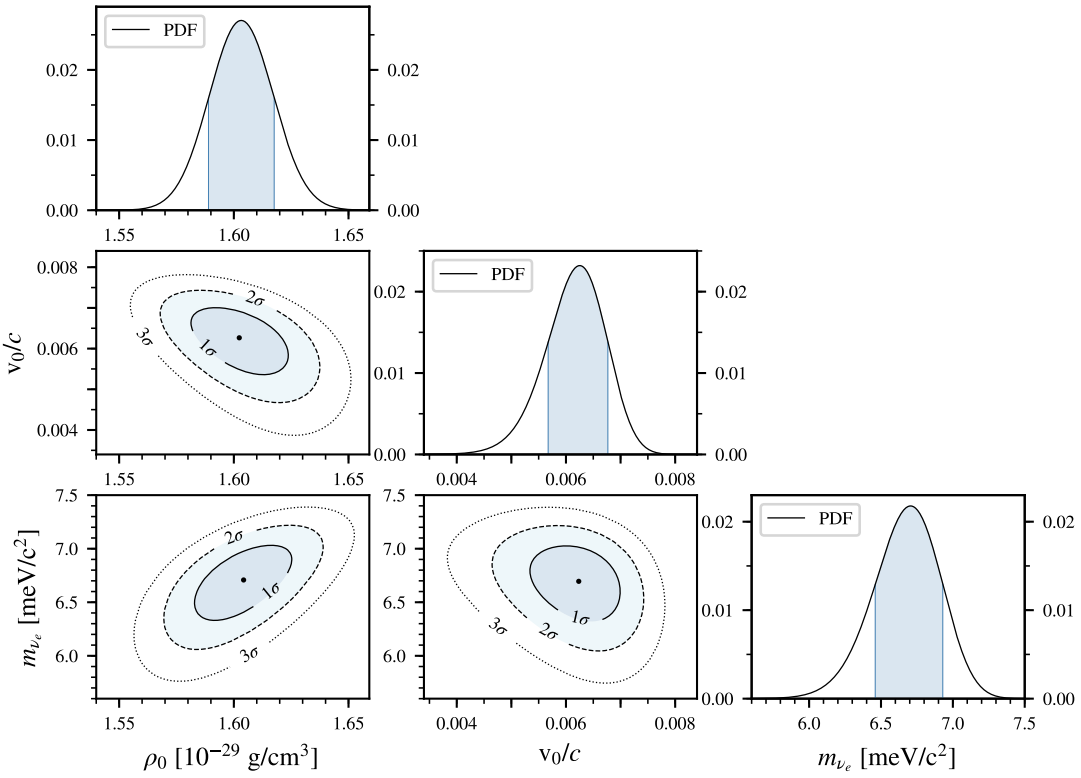

Figure 5. Likelihood contours for the central density (ρ_0) of the antineutrino star and the effective electron neutrino mass (m_{ν_e}). The SNe Ia data constrain the effective electron neutrino mass to high statistical precision, $m_{\nu_e} = 6.70 \pm 0.23$ meV/c^2. However, the systematic uncertainty associated with model assumptions likely dominates over the statistical uncertainty.

with a limiting radius of

$$\mathcal{R}_{\nu_e} = 15.1 \text{ Gly}, \tag{30}$$

which is consistent with the model of the early universe (see section 2.2). The re-formed antineutrino star has mass $M/\mathcal{M}_{\nu_e} = 0.855$ and radius $R_S/R = 0.410$ or

$$R = 21.1 \text{ Gly}. \tag{31}$$

Note that Chandrasekhar's equation of state for the above best-fit parameters naturally gives rise to these cosmological scales. Due to its large size, a degenerate antineutrino star can be detected by the large-scale motion of galaxies and an isothermal microwave background [19].

One can identify the best-fit value for the initial velocity $v_0 = 6.18 \pm 0.55 \times 10^{-3}$ as the root-mean-square speed of thermalized protons, since they are likely to be the most abundant matter particle by mass in the early universe. This would correspond to a proton temperature of $T_0 = 11.9 \pm 2.1$ keV, which is consistent with temperatures at which nucleosynthesis ends due to a decrease in fusion reaction rate with a decrease in density [48,49]. Moreover, this initial average expansion velocity is responsible for the difference between the ΛCDM model and the ATLAS model at low redshifts ($z < 0.04$). This difference corresponds to a faster average expansion rate at low redshifts than predicted by the ΛCDM model and could qualitatively explain the 4.4σ Hubble tension reported by Riess *et al.* [25,26] (see Fig. 3).

The best-fit parameters are also consistent with an antineutrino star that is degenerate, giving a central Fermi temperature $T_{F,0} = 34.1 \text{ K} > T_{CMB,0} = 2.73 \text{ K}$ [50]. However, the above values for R_S/R and T_{CMB}/T_F suggest that the systematic error due to model assumptions is $\sim 20\%$ and dominates over the statistical error. Future work could account for general relativistic effects $\mathcal{O}\left[(R_S/R)^2\right]$ and the temperature ratio T/T_F to improve the accuracy of the antineutrino star model. Since these effects are small and dominate at high-z, where supernova data is still sparse, they are ignored in the present model for simplicity.

The ATLAS model relies on testable assumptions, in particular on the assumption of negative gravitational mass. While there are strong theoretical arguments against negative gravitational mass (for a review, see [51]), there have not yet been any conclusive direct experimental tests. The assumption of negative gravitational mass is in principle testable on cosmological scales, galactic scales and laboratory scales. On cosmological scales, this assumption is consistent with observations as described above: (i) it allows for the formation of the first neutrino and antineutrino stars from a quantum vacuum state, and (ii) it accounts for the overall expansion of matter in the late universe. On galactic scales, it predicts detectable antimatter emission from hot accreting matter close to the event horizon of black holes [52,53]. For example, there exists a positron excess in the galactic center [54] and in cosmic rays [55–58], which could be emitted by accreting compact objects. On laboratory scales, several experiments are currently underway at the GBAR, ALPHA-g and AEGIS laboratories at CERN [59–61]. Using antiprotons from LHC operations, these experiments are able to produce antihydrogen and directly observe its motion in free fall. Therefore, laboratory experiments are currently underway to test a key assumption of the ATLAS model. In the event that experiments at CERN discover negative gravitational mass, the ATLAS model provides a helpful alternative to the ΛCDM model, which is not optimized for this contingency.

The ATLAS model can be empirically distinguished from the the ΛCDM model with a variety of other empirical tests, such as observations that challenge the ΛCDM model's assumption of isotropy and homogeneity on cosmological scales. For instance, observations of the largely isotropic Hubble expansion and small CMB dipole suggest that we are relatively close to, but not at, the exact center of the star. This off-center location could qualitatively explain anisotropies, such as hemispherical asymmetries in the power spectrum, detected at the $\sim 3\sigma$ level in the CMB [30]. These observations challenge the *isotropy* assumption of the ΛCDM model. In an effort to explain these observations,

many CMB anisotropies have been found to become less significant with the introduction of rotation (specifically, by using a Bianchi VII_h model, albeit one that is decoupled from the standard ΛCDM model) [30,62]. Future work could investigate whether this rotational axis in the CMB corresponds to the rotational axis of an antineutrino star.

Many CMB anisotropies, such as the hemispherical asymmetries, are predicted by the ATLAS model to disappear when viewed from rest at the *exact* center of the star. Therefore it may be possible to locate this central position with the study of CMB anisotropies alone. For example, the intersection of the axis of rotation found in the CMB with the plane on which hemispherical asymmetries are minimized could help locate the central region of the antineutrino star. Independently, this central region could coincide with an underdensity of matter in our cosmic neighborhood such as the so-called 'dipole repeller' at $z \approx 0.05$ [63]. The dipole repeller is a void that appears to have contributed to roughly half of our velocity (v_{CMB}) relative to the CMB [63]. If the center of the antineutrino star were indeed in our cosmic neighborhood ($z \lesssim 0.05$) and contributing significantly to v_{CMB}, then one would also expect to see an asymmetry in the expansion rate of nearby galaxies. Specifically, one would expect an asymmetry that is aligned with v_{CMB}. This is consistent with observations at the $\sim 2\sigma$ level of a dipole anisotropy in the distribution of nearby ($z \lesssim 0.1$) radio galaxies that is aligned with v_{CMB} [64,65].

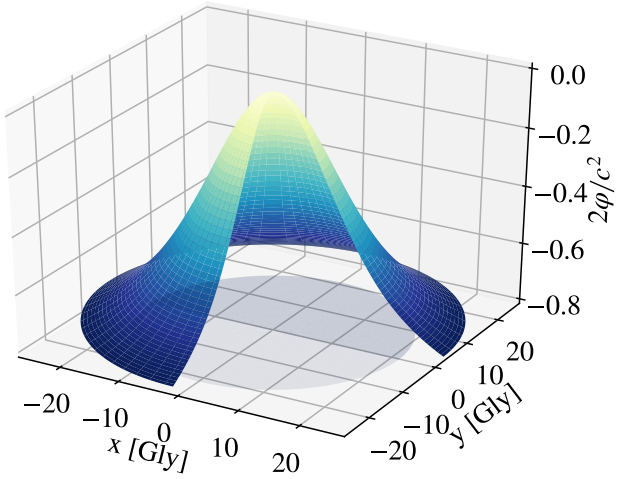

Figure 6. Surface plot of the gravitational potential in the equatorial plane of the antineutrino star. Solving Chandrasekhar's equation of state for the best-fit parameters gives a radius of cosmological scale, $R = 21.1$ Gly (*shaded area*). While baryonic test masses far from the core accelerate down the gravitational potential hill, observers initially at rest and close to the core will remain effectively at rest due to the relatively flat potential gradient here. Thus, the effect of an antineutrino star on galaxies viewed by central observers is comparable to the effect of a uniformly expanding metric.

As a further observational test, we note that galaxy clusters with redshifts in the range $0.5 \leq z \leq 2.5$ are moving at high velocities through the effectively stationary antineutrino gas whose density vanishes at $z \sim 2.5$ (see Fig. 4). The gravitational interaction between galaxy clusters and the antineutrino gas at rest could create conical acoustic shock waves that create circular thermal and density imprints in the CMB. This is qualitatively consistent with ring-shaped features found in the CMB [66,67]. More generally, one would expect the gravitational interaction between matter and the antineutrino star to generate correlations between the distribution of large scale structures for $z \lesssim 2.5$ and temperature fluctuations in the CMB.

Furthermore, recall that structure formation in the presented model of the early universe begins in a smaller volume for baryons than for antineutrinos due to their large mass difference (see Fig. 2). The initial baryonic structures will be relatively weakly bound and on a supercluster mass scale due to

their initially high temperature. As they continue their formation, these structures are dispersed by their acceleration in the gravitational potential of the antineutrino star (see Fig. 6). This is qualitatively consistent with the existence of large supercluster-size structures in the distant universe that are no longer gravitationally bound. For example, the Hercules-Corona Borealis Great Wall has been detected at the 1-3σ level with a size of 7-10 Gly [31,32]. This challenges the *homogeneity* assumption of the ΛCDM model, which predicts structures not larger than $\sim$ 1.21 Gly [68,69]. The ATLAS model appears qualitatively consistent with these observations, which may not yet seem significant when viewed individually, but collectively challenge the isotropy and homogeneity assumptions of the ΛCDM model.

Lastly, the ATLAS model proposes a possible origin of the big bang and dark energy, which are two major puzzles of the ΛCDM model. However, this work relies primarily on SNe Ia data to constrain its respective cosmological parameters (m_{ν_e}, ρ_0, v_0). This work is still at an early stage comparable to early work on the ΛCDM model [1–3]. During the twenty years since the discovery of dark energy, the ΛCDM model interpretation of SNe Ia data has been in general concordance with additional fits to observations such as baryon acoustic oscillations [4,70]. We do not attempt these fits yet; they are beyond the scope of the present work. This work provides a viable cosmological model for the contingency that ongoing experiments at CERN discover negative gravitational mass. The present work encourages future work to further develop and test the ATLAS model while relying on the ΛCDM model as a benchmark.

5. Conclusions

The entropy of the universe increases relative to an initial state of low entropy. A natural candidate for this initial state is the quantum vacuum. With the assumption that antimatter has negative gravitational mass, which is currently being tested at CERN, this vacuum gradually decays into neutrinos and antineutrinos. The collapse of an antineutrino star is a possible explanation for the energetic event commonly known as the big bang. After collapse and subsequent net creation of matter via baryogenesis, an antineutrino gas adiabatically expands and partially re-forms into an antineutrino star remnant in hydrostatic equilibrium. If viewed from its core, this star can today emit the isothermal CMB radiation and radially accelerate matter. This addresses the nature of dark energy, and removes the horizon and flatness problems without invoking cosmological inflation. The above ATLAS model is in good quantitative agreement ($\chi^2_\nu/\mathrm{dof} = 1.03$) with distance-redshift measurements. The electron neutrino mass is constrained as a cosmological parameter to $m_{\nu_e} = 6.70 \pm 0.23\,(\mathrm{stat.})\,\mathrm{meV/c^2}$. The model is qualitatively consistent with existing observations of large structures in the distant universe and anisotropies in the CMB. The presented alternative cosmological model is helpful for the contingency that ongoing experiments at CERN discover negative gravitational mass. Moreover, the apparent consistency of the presented model with observational data motivates future work to further develop and test the presented model while relying on the ΛCDM model as a benchmark.

Acknowledgments: The author gratefully thanks Mark Morris, Viktor Linders, Elizabeth Mills, Rainer Sachs, Ariella Machness and Troy Carter for helpful questions and comments on the manuscript. This work used computational resources associated with the Hoffman2 Shared Cluster provided by the UCLA Institute for Digital Research and Education.

References

1. A. Riess, A. Filippenko, P. Challis, A. Clocchiatti, A. Diercks, P. Garnavich, R. Gilliland, C. Hogan, S. Jha, R. Kirshner *et al.*. Observational Evidence from Supernovae for an Accelerating Universe and a Cosmological Constant. *The Astronomical Journal* **1998**, *116*, 1009. doi:10.1086/300499.
2. B. P. Schmidt, N. B. Suntzeff, M. M. Phillips, R. A. Schommer, A. Clocchiatti, R. P. Kirshner, P. Garnavich, P. Challis, B. Leibundgut, J. Spyromilio *et al.*. The High-Z Supernova Search: Measuring Cosmic Deceleration and Global Curvature of the Universe Using Type Ia Supernovae. *The Astrophysical Journal* **1998**, *507*, 46. doi:10.1086/306308.

3. S. Perlmutter, G. Aldering, G. Goldhaber, R. Knop, P. Nugent, P. Castro, S. Deustua, S. Fabbro, A. Goobar, D. Groom *et al.*. Measurements of Ω and Λ from 42 High-Redshift Supernovae. *The Astrophysical Journal* **1999**, *517*, 565–586. doi:10.1086/307221.
4. Huterer, D.; Shafer, D.L. Dark energy two decades after: observables, probes, consistency tests. *Rep. Prog. Phys.* **2018**, *81*, 016901. doi:10.1088/1361-6633/aa997e.
5. Ade, P. A. R. *et al.* (Planck Collaboration). Planck 2015 results - XIII. Cosmological parameters. *A&A* **2016**, *594*, A13. doi:10.1051/0004-6361/201525830.
6. Weinberg, S. The cosmological constant problem. *Rev. Mod. Phys.* **1989**, *61*, 1–23. doi:10.1103/RevModPhys.61.1.
7. Benoit-Lévy, A.; Chardin, G. Introducing the Dirac-Milne universe. *A&A* **2012**, *537*, A78. doi:10.1051/0004-6361/201016103.
8. Villata, M. On the nature of dark energy: The lattice Universe. *Astrophysics and Space Science* **2013**, *345*, 1–9. doi:10.1007/s10509-013-1388-3.
9. Hajdukovic, D.S. Virtual gravitational dipoles: The key for the understanding of the Universe? *Phys. Dark Univ.* **2014**, *3*, 34 – 40. doi:10.1016/j.dark.2014.03.002.
10. Manfredi, G.; Rouet, J.L.; Miller, B.; Chardin, G. Cosmological structure formation with negative mass. *Phys. Rev. D* **2018**, *98*, 023514. doi:10.1103/PhysRevD.98.023514.
11. Farnes, J. S.. A unifying theory of dark energy and dark matter: Negative masses and matter creation within a modified framework. *A&A* **2018**, *620*, A92. doi:10.1051/0004-6361/201832898.
12. Fardon, R.; Nelson, A.E.; Weiner, N. Dark energy from mass varying neutrinos. *J. Cosmology Astropart. Phys.* **2004**, *2004*, 005. doi:10.1088/1475-7516/2004/10/005.
13. Hoon, L.T. Degeneracy pressure of relic neutrinos and cosmic coincidence problem. *Can. J. Phys.* **2013**, *91*, 23–26. doi:10.1139/cjp-2012-0166.
14. Hartle, J.B.; Hawking, S.W. Wave function of the Universe. *Phys. Rev. D* **1983**, *28*, 2960–2975. doi:10.1103/PhysRevD.28.2960.
15. Khoury, J.; Ovrut, B.A.; Steinhardt, P.J.; Turok, N. Ekpyrotic universe: Colliding branes and the origin of the hot big bang. *Phys. Rev. D* **2001**, *64*, 123522. doi:10.1103/PhysRevD.64.123522.
16. Brandenberger, R.; Peter, P. Bouncing Cosmologies: Progress and Problems. *Found. Phys.* **2017**, *47*, 797–850. doi:10.1007/s10701-016-0057-0.
17. Sakharov, A.D. Violation of CP invariance, C asymmetry, and baryon asymmetry of the universe. *Sov. Phys. Uspekhi* **1991**, *34*, 392. doi:10.1070/PU1991v034n05ABEH002497.
18. Riotto, A.; Trodden, M. Recent Progress in Baryogenesis. *Annu. Rev. Nucl. Part. S.* **1999**, *49*, 35–75. doi:10.1146/annurev.nucl.49.1.35.
19. Penzias, A.A.; Wilson, R.W. A Measurement of Excess Antenna Temperature at 4080 Mc/s. *The Astrophysical Journal* **1965**, *142*, 419–421. doi:10.1086/148307.
20. Guth, A.H. Inflationary universe: A possible solution to the horizon and flatness problems. *Phys. Rev. D* **1981**, *23*, 347–356. doi:10.1103/PhysRevD.23.347.
21. Linde, A. A new inflationary universe scenario: A possible solution of the horizon, flatness, homogeneity, isotropy and primordial monopole problems. *Physics Letters B* **1982**, *108*, 389 – 393. doi:10.1016/0370-2693(82)91219-9.
22. Albrecht, A.; Steinhardt, P.J. Cosmology for Grand Unified Theories with Radiatively Induced Symmetry Breaking. *Phys. Rev. Lett.* **1982**, *48*, 1220–1223. doi:10.1103/PhysRevLett.48.1220.
23. Penrose, R. Difficulties with Inflationary Cosmology. *Annals of the New York Academy of Sciences* **1989**, *571*, 249–264. doi:10.1111/j.1749-6632.1989.tb50513.x.
24. Ijjas, A.; Steinhardt, P.J.; Loeb, A. Inflationary schism. *Physics Letters B* **2014**, *736*, 142 – 146. doi:10.1016/j.physletb.2014.07.012.
25. Riess, A.G.; Casertano, S.; Yuan, W.; Macri, L.; Anderson, J.; MacKenty, J.W.; Bowers, J.B.; Clubb, K.I.; Filippenko, A.V.; Jones, D.O.; Tucker, B.E. New Parallaxes of Galactic Cepheids from Spatially Scanning the Hubble Space Telescope: Implications for the Hubble Constant. *The Astrophysical Journal* **2018**, *855*, 136. doi:10.3847/1538-4357/aaadb7.
26. Riess, A.G.; Casertano, S.; Yuan, W.; Macri, L.M.; Scolnic, D. Large Magellanic Cloud Cepheid Standards Provide a 1% Foundation for the Determination of the Hubble Constant and Stronger Evidence for Physics beyond ΛCDM. *The Astrophysical Journal* **2019**, *876*, 85. doi:10.3847/1538-4357/ab1422.

27. Risaliti, G.; Lusso, E. Cosmological constraints from the Hubble diagram of quasars at high redshifts. *Nature Astronomy* **2019**. doi:10.1038/s41550-018-0657-z.
28. Chandrasekhar, S. The maximum mass of ideal white dwarfs. *The Astrophysical Journal* **1931**, *74*, 81. doi:10.1086/143324.
29. Chandrasekhar, S. The Highly Collapsed Configurations of a Stellar Mass. (Second Paper.). *Monthly Notices of the Royal Astronomical Society* **1935**, *95*, 207–225. doi:10.1093/mnras/95.3.207.
30. Ade, P. A. R. *et al.* (Planck Collaboration). Planck 2013 results. XXIII. Isotropy and statistics of the CMB. *A&A* **2014**, *571*, A23. doi:10.1051/0004-6361/201321534.
31. Horváth, I.; Hakkila, J.; Bagoly, Z. Possible structure in the GRB sky distribution at redshift two. *A&A* **2014**, *561*, L12. doi:10.1051/0004-6361/201323020.
32. Balazs, L.G.; Bagoly, Z.; Hakkila, J.E.; Horvath, I.; Kobori, J.; Racz, I.I.; Toth, L.V. A giant ring-like structure at 0.78<z<0.86 displayed by GRBs. *Monthly Notices of the Royal Astronomical Society* **2015**, *452*, 2236. doi:10.1093/mnras/stv1421.
33. Agostini, M. *et al.*. Improved Limit on Neutrinoless Double-β Decay of ^{76}Ge from GERDA Phase II. *Phys. Rev. Lett.* **2018**, *120*, 132503. doi:10.1103/PhysRevLett.120.132503.
34. Gando, A. *et al.*. Search for Majorana Neutrinos Near the Inverted Mass Hierarchy Region with KamLAND-Zen. *Phys. Rev. Lett.* **2016**, *117*, 082503. doi:10.1103/PhysRevLett.117.082503.
35. Fukuda, Y. *et al.* (Super-Kamiokande Collaboration). Evidence for Oscillation of Atmospheric Neutrinos. *Phys. Rev. Lett.* **1998**, *81*, 1562–1567. doi:10.1103/PhysRevLett.81.1562.
36. Ahmad, Q. R. *at al.* (SNO Collaboration). Direct Evidence for Neutrino Flavor Transformation from Neutral-Current Interactions in the Sudbury Neutrino Observatory. *Phys. Rev. Lett.* **2002**, *89*, 011301. doi:10.1103/PhysRevLett.89.011301.
37. Shapiro, S.L.; Teukolsky, S.A., Cold Equation of State Below Neutron Drip. In *Black Holes, White Dwarfs, and Neutron Stars*; John Wiley & Sons, Ltd, 2007; chapter 2, pp. 17–54. doi:10.1002/9783527617661.ch2.
38. Neiser, T.F. Cosmological implications of a degenerate antineutrino star. *American Astronomical Society* **2019**, *233*, 349.08.
39. Mertens, S. Status of the KATRIN Experiment and Prospects to Search for keV-mass Sterile Neutrinos in Tritium β-decay. *Physics Procedia* **2015**, *61*, 267 – 273. doi:10.1016/j.phpro.2014.12.043.
40. M. Aker *et al.*. An improved upper limit on the neutrino mass from a direct kinematic method by KATRIN. *arxiv:1909.06048* **2019**.
41. Schwinger, J. On Gauge Invariance and Vacuum Polarization. *Phys. Rev.* **1951**, *82*, 664–679. doi:10.1103/PhysRev.82.664.
42. Greiner, W.; Müller, B.; Rafelski, J., Quantum Electrodynamics of Strong Fields; Springer, Berlin, Heidelberg, 1985; p. 569. doi:10.1007/978-3-642-82272-8.
43. Alpher, R.A.; Bethe, H.; Gamow, G. The Origin of Chemical Elements. *Phys. Rev.* **1948**, *73*, 803–804. doi:10.1103/PhysRev.73.803.
44. A. Kogut, C. Lineweaver, G. F. Smoot, C. L. Bennett, A. Banday, N. W. Boggess, E. S. Cheng, G. de Amici, D. J. Fixsen, G. Hinshaw *et al.*. Dipole Anisotropy in the COBE Differential Microwave Radiometers First-Year Sky Maps. *The Astrophysical Journal* **1993**, *419*, 1. doi:10.1086/173453.
45. Radosz, A.; Augousti, A.; Ostasiewicz, K. Decoupling of Kinematical Time Dilation and Gravitational Time Dilation in Particular Geometries. *Acta Physica Polonica B* **2008**, *29*, 1357.
46. N. Suzuki, D. Rubin, C. Lidman, G. Aldering, R. Amanullah, K. Barbary, L. F. Barrientos, J. Botyanszki, M. Brodwin, N. Connolly *et al.*. The Hubble Space Telescope Cluster Supernova Survey. V. Improving the Dark-energy Constraints above $z > 1$ and Building an Early-type-hosted Supernova Sample. *The Astrophysical Journal* **2012**, *746*, 85. doi:10.1088/0004-637X/746/1/85.
47. Esteban, I.; Gonzalez-Garcia, M.C.; Maltoni, M.; Martinez-Soler, I.; Schwetz, T. Updated fit to three neutrino mixing: exploring the accelerator-reactor complementarity. *J. High Energy Phys.* **2017**, *2017*, 87. doi:10.1007/JHEP01(2017)087.
48. Bosch, H.S.; Hale, G. Improved formulas for fusion cross-sections and thermal reactivities. *Nuclear Fusion* **1992**, *32*, 611. doi:10.1088/0029-5515/32/4/I07.
49. Wesson, J. *Tokamaks*, 4th ed.; International series of monographs, Oxford Univ. Press: Oxford, 2011; pp. 7–8.
50. Fixsen, D.J. The Temperature of the Cosmic Microwave Background. *The Astrophysical Journal* **2009**, *707*, 916. doi:10.1088/0004-637X/707/2/916.

51. Nieto, M.M.; Goldman, T. The arguments against "antigravity" and the gravitational acceleration of antimatter. *Phys. Rep.* **1991**, *205*, 221 – 281. doi:10.1016/0370-1573(91)90138-C.
52. Hajdukovic, D.S. Can the New Neutrino Telescopes Reveal the Gravitational Properties of Antimatter? *Advances in Astronomy* **2011**, *2011*. doi:10.1155/2011/196852.
53. Villata, M. The matter-antimatter interpretation of Kerr spacetime. *Ann. Phys. (Berlin)* **2015**, *527*, 507–512. doi:10.1002/andp.201500154.
54. Weidenspointner, G.; Skinner, G.; Jean, P.; Knödlseder, J.; von Ballmoos, P.; Bignami, G.; Diehl, R.; Strong, A.W.; Cordier, B.; Schanne, S.; Winkler, C. An asymmetric distribution of positrons in the Galactic disk revealed by γ-rays. *Nature* **2008**, *451*, 159 EP –. doi:10.1038/nature06490.
55. O. Adriani *et al.*. Cosmic-Ray Positron Energy Spectrum Measured by PAMELA. *Phys. Rev. Lett.* **2013**, *111*, 081102. doi:10.1103/PhysRevLett.111.081102.
56. L. Accardo *et al.*. High Statistics Measurement of the Positron Fraction in Primary Cosmic Rays of $0.5 - 500$GeV with the Alpha Magnetic Spectrometer on the International Space Station. *Phys. Rev. Lett.* **2014**, *113*, 121101. doi:10.1103/PhysRevLett.113.121101.
57. M. Aguilar *et al.*. Antiproton Flux, Antiproton-to-Proton Flux Ratio, and Properties of Elementary Particle Fluxes in Primary Cosmic Rays Measured with the Alpha Magnetic Spectrometer on the International Space Station. *Phys. Rev. Lett.* **2016**, *117*, 091103. doi:10.1103/PhysRevLett.117.091103.
58. Abeysekara, A. U. *et al.*. Extended gamma-ray sources around pulsars constrain the origin of the positron flux at Earth. *Science* **2017**, *358*, 911–914. doi:10.1126/science.aan4880.
59. P. Pérez, D. Banerjee, F. Biraben, D. Brook-Roberge, M. Charlton, P. Cladé, P. Comini, P. Crivelli, O. Dalkarov, P. Debu *et al.*. The GBAR antimatter gravity experiment. *Hyperfine Interact.* **2015**, *233*, 21–27. doi:10.1007/s10751-015-1154-8.
60. The ALPHA Collaboration & A. E. Charman. Description and first application of a new technique to measure the gravitational mass of antihydrogen. *Nat. Commun.* **2013**, *4*, 1785 EP –. doi:10.1038/ncomms2787.
61. R. S. Brusa, C. Amsler, T. Ariga, G. Bonomi, P. Bräunig, L. Cabaret, M. Caccia, R. Caravita, F. Castelli, G. Cerchiari *et al.*. The AEgIS experiment at CERN: measuring antihydrogen free-fall in earth's gravitational field to test WEP with antimatter. *Journal of Physics: Conference Series* **2017**, *791*, 012014. doi:10.1088/1742-6596/791/1/012014.
62. Ade, P. A. R. *et al.* (Planck Collaboration). Planck 2013 results. XXVI. Background geometry and topology of the Universe. *A&A* **2014**, *571*, A26. doi:10.1051/0004-6361/201321546.
63. Hoffman, Y.; Pomarède, D.; Tully, R.B.; Courtois, H.M. The dipole repeller. *Nat. Astron.* **2017**, *1*, 0036 EP –. doi:10.1038/s41550-016-0036.
64. Singal, A.K. Large Peculiar Motion of the Solar System from the Dipole Anisotropy in Sky Brightness due to Distant Radio Sources. *The Astrophysical Journal Letters* **2011**, *742*, L23. doi:10.1088/2041-8205/742/2/L23.
65. Tiwari, P.; Nusser, A. Revisiting the NVSS number count dipole. *J. Cosmology Astropart. Phys.* **2016**, *2016*, 062. doi:10.1088/1475-7516/2016/03/062.
66. Gurzadyan, V.G.; Penrose, R. On CCC-predicted concentric low-variance circles in the CMB sky. *The European Physical Journal Plus* **2013**, *128*, 22. doi:10.1140/epjp/i2013-13022-4.
67. An, D.; Meissner, K.A.; Nurowski, P. Ring-type structures in the Planck map of the CMB. *Monthly Notices of the Royal Astronomical Society* **2018**, *473*, 3251–3255. doi:10.1093/mnras/stx2299.
68. Yadav, J.K.; Bagla, J.S.; Khandai, N. Fractal dimension as a measure of the scale of homogeneity. *Monthly Notices of the Royal Astronomical Society* **2010**, *405*, 2009–2015. doi:10.1111/j.1365-2966.2010.16612.x.
69. Clowes, R.G.; Harris, K.A.; Raghunathan, S.; Campusano, L.E.; Söchting, I.K.; Graham, M.J. A structure in the early Universe at $z \sim 1.3$ that exceeds the homogeneity scale of the R-W concordance cosmology. *Monthly Notices of the Royal Astronomical Society* **2013**, *429*, 2910–2916. doi:10.1093/mnras/sts497.
70. Ruiz-Lapuente, P.; Bassett, B.; Hlozek, R., Baryon acoustic oscillations. In *Dark Energy: Observational and Theoretical Approaches*; Cambridge University Press: Cambridge, 2010; pp. 246–278. doi:10.1017/CBO9781139193627.010.